Solar Energy Materials & Solar Cells 149 (2016) 29–39

Contents lists available at ScienceDirect

Solar Energy Materials & Solar Cells

journal homepage: www.elsevier.com/locate/solmat

Performance enhancement of a Building-Integrated Concentrating Photovoltaic system using phase change material

Shivangi Sharma [a,*], Asif Tahir [a], K.S. Reddy [b], Tapas K. Mallick [a,*]

[a] Environmental and Sustainability Institute, University of Exeter, Penryn Campus, Cornwall TR109FE, UK
[b] Heat Transfer Laboratory, IIT Madras, Chennai, India

ARTICLE INFO

Article history:
Received 13 November 2015
Accepted 29 December 2015
Available online 21 January 2016

Keywords:
Building-Integrated Concentrating Photovoltaics (BICPV)
Phase Change Materials (PCM)
Concentrating Photovoltaics (CPV)
Solar energy

ABSTRACT

Building-Integrated Concentrated Photovoltaic (BICPV) systems integrate easily into built environments, replacing building material, providing benefits of generating electricity at the point of use, allowing light efficacy within the building envelope and providing thermal management. This paper presents a novel experimental evaluation of phase change materials (PCM) to enhance performance of low-concentration BICPV system via thermal regulation. Previous studies have primarily focussed on temporal and spatial studies of PCM temperature within the BIPV systems but the current work also discusses the effect of PCM on electrical parameters of the BICPV systems. Due to the inadequacy of the earlier reported model, a new analytical model is proposed and implemented with the in-house controlled experiments. Paraffin wax based RT42 was used within an in-house designed and fabricated PCM containment. An indoor experiment was performed using highly collimated continuous light source at 1000 W m^{-2}. Results show an increase in relative electrical efficiency by 7.7% with PCM incorporation. An average reduction in module centre temperature by 3.8 °C was recorded in the BICPV–PCM integrated system as compared to the naturally ventilated system without PCM. Studies showed that PCM effectiveness varies with irradiance; an increase in relative electrical efficiency by 1.15% at 500 W m^{-2}, 4.20% at 750 W m^{-2} and 6.80% at 1200 W m^{-2} was observed.

1. Introduction

Building-Integrated photovoltaics (BIPV) is proving to be the most rapidly emerging technology within the solar industry globally with an estimated capacity growth of about 50% or more from 2011 to 2017 [1]. Some of its applications are found in a shading device for windows, semi-transparent glass façade, building exterior cladding panel and parapet unit or roofing system [2]. Building-Integrated Concentrated Photovoltaic (BICPV) systems concentrate solar radiation with the help of curved mirrors (reflective-types), concentrators or lenses (refractive-types). They offer advantages over conventional flat panel BIPV systems in improved electrical conversion efficiency, better use of space, option of recycling the component materials and use of less toxic products associated with production of PV cells [3]. Concentrators with low geometrical concentration ratios ($C_g < 10\times$ concentrations) are mostly static in nature providing simplicity in building integration and design [4].

BICPV systems face challenge with rise in temperature, manifested as electrical efficiency loss and overheating. Therefore, cooling of modules is essential and is currently achieved via natural air circulation in fins and heat spreaders [5]. The efficiency loss with rising temperature in a PV module is mainly due to a decrease in open-circuit voltage (V_{OC}), which has negative temperature coefficient [6]. Low-cost silicon based solar cells convert a small (less than 20%) portion of the sunlight to electricity [7]. The remaining photons are dissipated in the cells as heat. Due to high local solar power density, non-converted solar energy flux is almost evenly redistributed inside the heat sink [8]. Efficiency of silicon cells reduces at a rate of approximately 0.45% per degree increase in temperature [9]. Along with temperature control, uniformity of temperature throughout the panel is desirable to avoid hot spots, which may give rise to current mismatch and reduction in overall system efficiency [10].

Recently emerging integration of Photovoltaic (PV) and phase change materials (PCMs) system concept for temperature control offers an opportunity for extending its usage to BICPV systems. Employing PCMs passively retain the BICPV temperature within safe operating zone and can also collect rejected heat for possible regeneration. PCMs are materials that absorb and release heat energy in the latent form during phase transitions over a narrow

* Corresponding authors. Tel.: +44 1326 259478.
E-mail addresses: ss664@exeter.ac.uk (S. Sharma), A.Tahir@exeter.ac.uk (A. Tahir), ksreddy@iitm.ac.in (K.S. Reddy), T.K.Mallick@exeter.ac.uk (T.K. Mallick).

http://dx.doi.org/10.1016/j.solmat.2015.12.035

Nomenclature

A	front surface area of the system (m^2)
I	irradiance on photovoltaic ($W\,m^{-2}$)
h_1, h_2	heat transfer coefficient at front and rear surface ($W\,m^{-2}\,K^{-1}$)
Δx	depth of the BIPV-PCM system (m)
η_{elec}	electrical efficiency of the solar cell
C_g	geometrical (concentration ratio) of the concentrator (collector aperture area/receiver surface area)
T_{amb}	ambient temperature (°C)
T_m	PCM melting peak temperature (°C)
T_c	Module central temperature (°C)
$T_{PV,t}$–$T_{PCM,top}$	temperature on PV at time t which is also the top plate temp PCM (°C)
$T_{PV,\ t+\Delta t}$	temperature on PV at time $t+\Delta t$ (°C)
$T_{PCM,bottom}$	temperature on PCM bottom plate (°C)
C_P	specific heat of PCM ($J\,kg^{-1}\,K^{-1}$)
ρ	density of PCM ($kg\,m^{-3}$)
k	thermal conductivity ($W\,m^{-1}\,K^{-1}$)
H	latent heat of PCM ($J\,kg^{-1}$)
Δt	time step (s)
t	time (s)
Qs	heat energy stored in the PCM ($J\,kg^{-1}$)
I_{SC}	short circuit current (mA)
V_{OC}	open circuit voltage (V)
P_m	maximum electrical power output (mW)

temperature range or at nearly constant temperatures [11], thus their heats of fusion can buffer temperature variations [12]. PCMs find applications in thermal management of buildings for higher energy efficiency by integrating with building masonry [13] and as thermal energy storage systems for solar water heating application [14] etc. Specifically, they may be used in macro-encapsulated form into the ventilated façade in its air cavity for daylighting and room heating [15], for low-energy and free cooling of buildings [16,17], as lightweight thermally activated ceiling panels [18], as moving PCM curtains integrated with thermally effective windows [19], to impart improvement in hot water heat stores with stratification [20], as tiles for building use [21], floor supply air conditioning system with thermal energy storage using granulated PCM [22] etc. PCMs were also used for capacitance in the air conditioning systems for reducing fluctuations in the daily cooling load, which later developed into direct integration with the refrigeration systems to save energy and for better control [23]. PCMs may be broadly classified as organic, inorganic and eutectics and the classification has been briefly summarised in Fig. 1.

Operational advantages of PCMs in latent heat storage systems over sensible heat storage (SHS) systems, such as water, include smaller temperature fluctuations due to reduced temperature difference between charging and discharging heat cycles, smaller size and weight per unit of storage capacity, high energy density (typically 5–14 times of SHS for a given working temperature range), reliability, and flexibility [24]. The drawbacks of using these systems, however, are that PCMs, especially organic ones, exhibit very low thermal conductivity and that solid to gas and liquid to gas phase transformations are associated with high volumetric changes [25]. Undesirable material property changes due to cycling, phase segregation and sub-cooling calls for further analysis before implementing PCMs [26]. Leakage of PCM in melted state also poses practical limitation to their successful application in various systems.

Encapsulation or using shape-stabilization, prepared by PCM integration into supporting material and microencapsulating PCMs in shells could potentially solve PCM leakage issues. These shape-stabilized PCMs can be categorised as composite PCMs and microencapsulated PCMs [27]. HDPE (high-density polyethylene) material, formed stable via cross-linking, has been frequently employed as a PCM supporting material due to its high structural strength.

Possible remedy to address low thermal conductivity include improved heat transfer techniques to increase charging, discharging rates and addition of high thermal conductivity materials. Traditionally used metal inserts with paraffin wax (reported since 1966) are Aluminium (forms such as honeycomb, powder, gauze, fins, alumina foam and powder etc.), Copper (Cu foam, plates used as circular and longitudinal fin etc.), stainless steel (screens, spheres, fin etc.), carbon fibre (woven sheets and brushes etc.) and graphite (powder, expanded, exfoliated, matrix etc.) [28]. Composite PCMs with fillers also prove to be more thermally conductive [28]. Experimentally, composite PCM thermal conductivity improvement of 14% (with T_m=42–44 °C) and 24% (T_m=56–58 °C) have been achieved using expanded and exfoliated graphite (EG) (ratio of 3% by mass) owing to the thermally conductive network of the EG pore structure [29]. Further, the thermal conductivities of the composite PCMs varied linearly (with a high-correlation of r=0.9986) with the mass fraction of the conductivities enhancement material, EG in this case. An increase of 81.2%, 136.3%, 209.1%, and 272.7% thermal conductivity in composite PCM was noticed using 2%, 4%, 7%, and 10% mass fraction respectively as compared to plain paraffin wax [30].

Selection of PCMs can be broadly based on the following physical, thermal and chemical properties including concerns for the environment, economics and safety criterion: (a) phase change temperature (PCT) falling within the desired range [26]; (b) high latent heat, specific heat and thermal conductivity [31]; (c) Low-volume expansion and low/no sub-cooling during freezing [32]; (d) non-poisonousness, non-corrosiveness, non-flammable, non-explosive and chemically stable [26]; and (e) low-cost. Selection criterion may include full or partial storage availability, freezing, melting heat transfer characteristics and reliability in cyclic duty [33]. PCMs selection for specific BICPV systems may be based on concentration method and level, available irradiance, geometry of the system, operating temperature of silicon cells and containment material and design. Additionally, charging/discharging rates, heat exchanging surface and thermal conductivity of heat exchange container material play a vital role [34].

This paper details the results of a preliminary experimental investigation performed on an in-house manufactured BICPV module using dielectric based linear asymmetric compound parabolic concentrator designed by the authors of [35]. Despite extensive literature is available for BICPV systems, no experimental work with PCM cooling application has been reported so far. The aims of the experiment were to design and fabricate the integrated BICPV–PCM module and target heat captivation and cooling of the BICPV side by the PCM for improved electrical efficiency. Further, it was aimed to experimentally quantify and compare the electrical efficiency improvement achieved with the same PCM at varying irradiance levels in a controlled indoor environment. Thermal regulation provided by an organic paraffin wax based PCM (RT 42®) and its effect on module's electrical performance were tested under ambient temperature conditions (15–25 °C) and relative humidity between 24% and 36%. The four different irradiance levels are selected as 500, 750, 1000 and

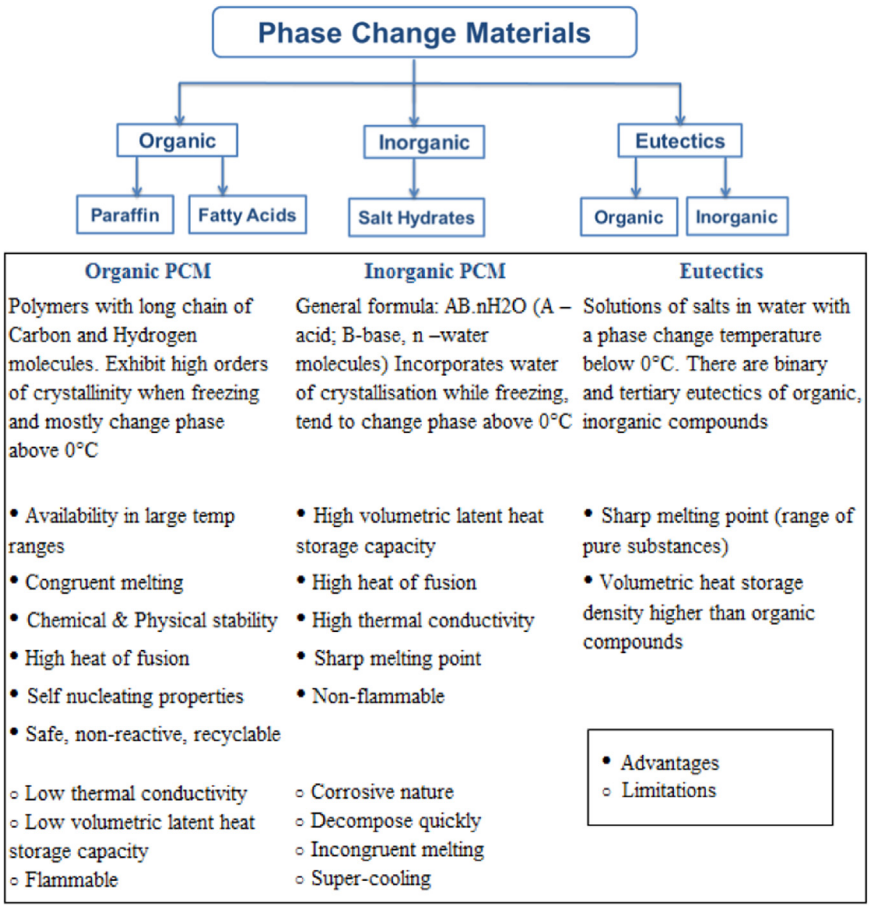

Fig. 1. Broad classification of PCM; their advantages and limitations.

1200 W m^{-2} to cover a broad range of intensity for testing PCM efficacy. Organic PCMs based on paraffin wax has been selected for this study due to their high latent heat of fusion, very insignificant amount of super-cooling, chemical non-reactiveness, low vapour pressure, self-nucleating properties, environment friendliness, non-toxicity, no phase segregation and low-cost.

1.1. Literature review

Previous relevant work for the BICPV systems could be referred to from the following literature: the authors of [36] designed and experimentally characterized the novel non-imaging asymmetric compound parabolic photovoltaic concentrator. They characterised the BICPV system with and without concentrators under outdoor conditions in Northern Ireland (54°36′N, 5°37′W). The thermal and electrical analysis was carried out for 20 days with an average of 10 h each day. The results revealed an increase in the PV module maximum power point by 62% with concentration as compared to the one without concentration. Sarmah et al. [35] further designed, developed and analysed indoor performance of a BICPV module made with clear polyurethane linear dielectric concentrator and eight silicon solar cells in series (1.89W_p) under different incidence angles. Their concentrator design differed from the previously designed counterpart with acceptance-half angles as 0° and 33° (0° and 50° for the former) and concentration ratio 2.8 (2.0 formerly). Average AM1.5G spectrum weighted transmittance (in spectral range 300–1100 nm) for the concentrator was 81.9%. Indoor characterisation using solar simulator (1000 W m^{-2} at 20° inclination) resulted in maximum power ratio of 2.27 compared to the non-concentrating system. Within the designed concentrator's acceptance angle range, 80.5% optical efficiency, 12.1% maximum and 9.43% average electrical conversion efficiency was achieved. Additionally, these BICPV systems achieved 20% cost reduction (£0.80 for PV and £0.64 for CPV for 1 kW system) calculated on per unit power output basis. Baig et al. [37] further developed the numerical model for the system and performed experimental validation considering concentration ratios, solar cell material properties, operating temperatures, solar cell dimensions, bus bar configuration, number of fingers, their size and spacing. Issues with concentrated irradiance such as non-uniformity of the incident flux, hot spots, current mismatch and efficiency reduction were considered for simulation. It was found that non-uniformity in illumination accounts for around 0.5% loss in absolute electrical efficiency and a relative fill factor loss of 1.85% at 5° incident angle. Ray tracing and finite element methods were employed to carry out the optical analysis and electrical and thermal analysis respectively. The difference in P_m between numerical model (262.6 mW) and experiment results (231.6 mW) was 11.4% which was attributed to the inherent defects in the concentrator (optical) and solar cell, misalignments between cell and concentrator, junction temperature difference causing V_{OC} variation, current mismatch between series connected cells and modelling constants used in the electrical model.

The authors of [38], with their broad review of energy storage methods, investigated and analysed latent heat storage materials (thermal, physical, kinetic and chemical properties and economics) such as PCM. They categorised PCM as group I (most promising), group II (promising) and group III (less promising; with insufficient data) based on properties such as T_m and H and number of carbon atoms. Measurement techniques for T_m and H, based on differential thermal analysis (DTA) and differential scanning calorimetry (DSC) using alumina as the reference material are also

discussed in brief. Thermo-physical properties (thermal conductivity, density and specific heat) of several PCM containment materials such as Aluminium, copper, glass, stainless steel etc. are presented. Numerical simulation of latent heat storage systems, enthalpy formulation and numerical solution for the moving boundary or Stefan problem has been suggested and solved using algebraic equations using the control volume technique developed by Voller [39] and Patankar [40]. An interesting concept of off-peak electricity storage [41] wherein PCMs are melted to stock surplus electricity as latent heat energy providing hotness/coldness when required, which can reduce peak load requirements and uniformalise electricity demand, thereby achieving cost reduction.

In a study on BIPV–PCM system, a 1-D dynamic simulation programme developed with MATLAB/SIMULINK® and solved using control-volume based finite-difference scheme, the electrical and thermal efficiency showed respective increase of 10% and 12%, with experimental and numerical results in agreement [42]. The authors of [43] reviewed PCM utilisation for thermal management of concentrating and non-concentrating PV modules. The effect of temperature rise on different PV systems, comparison between hybrid photovoltaic thermal (PV/T)–PCM and PV–PCM systems, commercialisation, practical use, economics of incorporating PCM with PV systems, various experimental set up of PV–PCM systems and results as given in literature and number of studies reported since 1978 through to 2014 have been discussed. PCM cooling techniques for PV systems could assume passive or active mode with heat regeneration achieved by natural cooling and active heat removal respectively. They concluded that by and large, the use of PCM contributes to performance improvement of such systems. However, the studies were performed for short durations and require testing for extended periods of time to understand the discharging and re-charging of PCM, as full-discharge becomes indispensable for its maximum heat storage capacity during the next charging cycle.

PCMs use for thermal regulation of BIPV have been experimentally reported in [44], for a PV–PCM system that achieved maximum temperature reduction of 18 °C for 30 min and of 10 °C for 300 min at an irradiance of 1000 W m^{-2}. A selection of five different PCMs (commercially available paraffin wax; RT20, eutectic mixture of Capric–Lauric acid and Capric–Palmitic acid, a pure salt hydrate; $CaCl_2 \bullet 6H_2O$, and a commercial blend); SP22 (all with T_m, 21–29 °C and H, 140–213 kJ/kg) were used to experiment at three irradiance levels (500, 750 and 1000 W m^{-2}) to evaluate the performance of each PCM. Variable parameters for the experiment were thermal conductivity and mass of the PCM and were achieved by altering container materials (Aluminium and Perspex), dimensions (width) and quantity. Four types of PCM containments were fabricated using Aluminium and Perspex with 3 cm and 5 cm width each. In general, all PCM containments made with Aluminium (5 cm) outperformed Perspex based ones at all irradiance levels. For warm climates (T_{amb} around 34 °C, I=1000 W m^{-2}), PV–PCM systems with Capric–Palmitic acid and $CaCl_2 \bullet 6H_2O$ were found economically viable. The results from [44] could be summarised in terms of the degree (temperature difference) and duration of deviation (time difference) between the BIPV surface temperature without and with PCM, as summarised in Table 1.

In another series of studies, Huang et al. [45] demonstrated the substantial effect of temperature regulation on PV efficiency improvement. Three configurations initially tested were (i) single flat Aluminium plate system, (ii) PV–PCM without internal fins and (iii) PV–PCM with internal fins using PCM RT25. A 0.0045 m thick Aluminium plate was used to fabricate the PCM containment with inner dimensions (L=0.300 m, W=0.040 m, H=0.132 m) and two full-length 0.030 m wide fins. The system (iii) maintained front surface temperature below 36.4 °C for 80 min with one PCM (T_m – 32°C, depth 20 mm) under 1000 W m^{-2} irradiance, (T_{amb} – 20 °C), while it was below 33 °C for 150 min with another PCM (T_m – 26.6 °C, depth 40 mm) under 750 W m^{-2} irradiance. Provision of metal fins within the PCM containment also showed significant thermal performance improvement. Another experiment by the same author [46], evaluated the performance of two PCMs (paraffin wax based RT25, granulated; GR40) for limiting temperature elevation of PV systems achieved temperature reduction of over 30 °C using RT25 with internal fins. Four sets of systems were characterised at 750 W m^{-2} (T_{amb} 23 ± 1 °C), namely; (i) flat Aluminium plate, (ii) flat Aluminium plate with eleven fins at (width 27 mm, thickness 0.5 mm thick and 12 mm pitch), (iii) PV–PCM system and (iv) PV–PCM system with thirty one Aluminium fins (40 mm inside the PCM) with RT25. The effect of fin parameters on temperature control could be summarised as:

(i) Fin spacing – five fin spacing (4, 8, 12, 16, 20 mm were studied) in vertical orientation and showed that 8 mm spacing nearly halves the number of fins required as compared to 4 mm spacing and also maintains the temperature under 28 °C by accommodating larger amount of PCM. The 4 mm spaced systems were the quickest to melt lowering the front surface temperature due to higher heat transfer rate. The temperature difference between fin spacing of 12 and 4 mm was only 0.9 °C. The best configuration with 8–12 mm space used smaller amount of fin material and sustained lower temperature for extended periods.

(ii) Fin width – out of the studied five fin widths (27, 30, 33, 36, 40 mm), the 40 mm ones performed the best in maintaining PV frontal surface at 28 °C for the longest duration (125 min). The relation between the fin width and temperature retaining time was almost linear exception being the widths of 30 and 33 mm that displayed insignificant effect.

(iii) Fin types – three types of fins (strip Aluminium matrix, uncoated soft-iron wire matrix and straight fins of 36 mm width) were chosen to study the effect of fin types and the lattermost reached the least temperature with fastest phase change completion.

The experimental results, numerical simulation and reviews discussed in this section underline the effectiveness of PCMs in electronic components cooling, for regulating photovoltaic temperatures and pave a way for further introductory application into BICPV systems.

Table 1
Degree and deviation in 4 h period for various PCMs applied to the BIPV system (data source [44]).

Irradiance	PCM→	RT20	Capric–Lauric acid	Capric–Palmitic acid	$CaCl_2 \bullet 6H_2O$	SP22
500 W/m^2	Degree (°C)	4.6	7	7.5	8	6.5
	Duration (h)	6.5	9	11.0	13	9.5
750 W/m^2	Degree (°C)	7.5	8	9.0	10	7.5
	Duration (h)	6.0	8	10.0	12	9.0
1000 W/m^2	Degree (°C)	3.5	4	11.0	12	7.5
	Duration (h)	5.5	6	9.5	11	9.0

2. Experimental design and manufacturing of the BICPV–PCM system

2.1. Design of the BICPV–PCM system

The manufactured BICPV module is shown in Fig. 2(a) while the details of geometrical design of the linear asymmetric compound

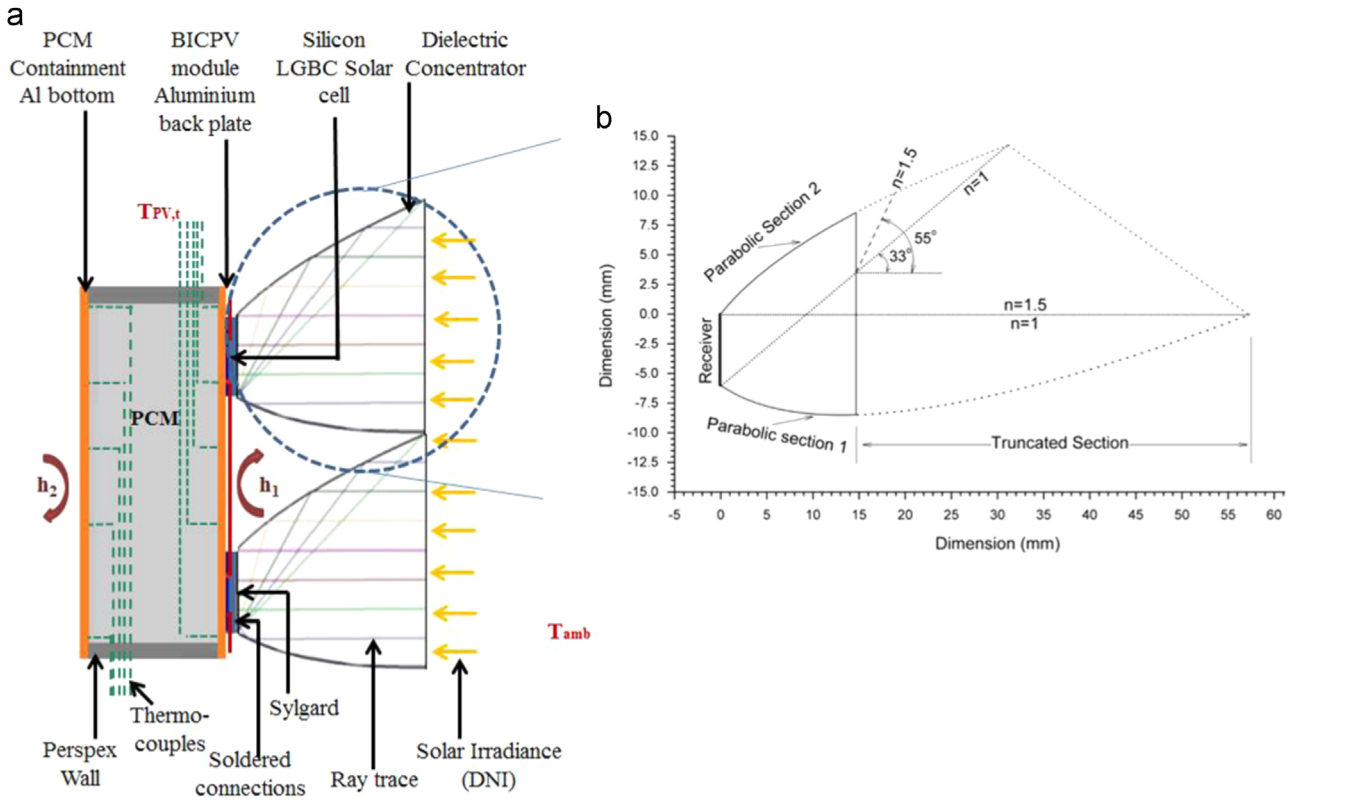

Fig. 2. (a) Side view of the fabricated BICPV–PCM system (not drawn to scale and inclined vertically for representation) and (b) geometrical design of a linear asymmetric compound parabolic concentrator (adapted from [35]).

parabolic concentrator (LACPC) with acceptance half-angles (0° and 55°) are shown in Fig. 2(b). The test prototype of the PCM containment/heat sink was developed using 13 mm thick Perspex sheet walls with the inner dimensions of $144 \times 134 \times 38$ mm^3 and outer dimensions of $170 \times 160 \times 42$ mm^3. The Aluminium back plate (0.6 mm thickness) of the BICPV system acts as the top covering for the PCM containment while another Aluminium plate of same thickness supports the bottom as its base. This design was based on modified heat transfer equations as expressed in Eqs. (5) and (6) given below. As per the available literature [45], the energy balance for a BIPV–PCM system is defined as follows:

(a) For TPV, $t < T_m$, the relation is given by

$$AI\Delta t = A(h_1 + h_2)(T_{PV,t} - T_{amb})\Delta t + (T_{PV,t} - T_{PV,t})\rho C_p \Delta x A \quad (1)$$

(b) The energy balance for the phase transition is

$$AI\sum \Delta t = A(h_1 + h_2)(T_m - T_{amb})\Delta t + H\Delta x A \quad (2)$$

The assumptions being:

i) Initial thermal equilibrium between the BIPV and PCM
ii) Constant values of h_1 and h_2
iii) Top and bottom adiabatic boundaries of the system

These equations seem mathematically inconsistent for the reasons stated below.

a. Eq. (2) is dimensionally unbalanced in its last term, which could be balanced by taking density of PCM is taken into consideration and the variable, area (A) could be eliminated from the equation, essentially which means the equation could take the form of (3) and (4)

$$I\Delta t = (h_1 + h_2)(T_{PV,t} - T_{amb})\Delta t + (T_{PV,t+\Delta t} - T_{PV,t})\rho C_p \Delta x A \quad (3)$$

$$I\sum \Delta t = (h_1 + h_2)(T_m - T_{amb})\Delta t + \rho H \Delta x \quad (4)$$

b. This energy transfer does not consider the electrical conversion efficiency of the solar cell (typically 16–20%), implying conversion of 100% of the available solar irradiance into heat and no useful electrical conversion taking place within the BIPV system.

c. An alternate energy balance equation for the BICPV system, considering it as a transient heat transfer case in a 1D domain, making an allowance for the geometrical concentration of the concentrator, could be written as (5) and (6). The term ($1-\eta_{elec}$) signifies that part of irradiance which is not converted to electricity, (typically 80% of the available irradiance).

These are based on the assumptions as stated above (i) - (iii) and also that

(iv) The PCM is immiscible, non-reactive and homogeneous
(v) The heat transfer occurs primarily by natural convection and heat conduction
(vi) Radiation losses and thermal resistance between the PCM and walls and between PCM and PV are neglected

Therefore, the modified equations are proposed as follows:

$$I(1-\eta_{elec})C_g\Delta t = (h_1 + h_2)(T_{PV,t} - T_{amb})\Delta t + (T_{PV,t+\Delta t} - T_{PV,t})\rho C_p \Delta x \quad (5)$$

$$I(1-\eta_{elec})C_g \sum \Delta t = (h_1+h_2)(T_m-T_{amb})\Delta t+\rho H\Delta x \quad (6)$$

These equations may form the base of heat transfer studies in BICPV–PCM systems, a 3D control volume based on heat flow perpendicular to the irradiance assuming no heat transfer takes place in the walls due to extremely low thermal conductivity (0.1875 W m^{-1} K^{-1}) of perspex.

2.2. Material and manufacturing process of BICPV–PCM system

Low-concentrating LACPC concentrators ($C_g \sim 2.7$ due to manufacturing limitations and shrinkage) were manufactured using optically clear liquid *Crystal Clear® 200 Clear Urethane Casting Resin* (two-part, with 10:9 mix ratio) as reported by Sarmah et al. [35]. Five LGBC (Laser Grooved Buried Contact) crystalline silicon cells with dimensions 116×6 mm^2 were soldered in series connection using thin tin-plated copper strips. This module was assembled on Aluminium back plate for ensuring good thermal conduction; wrapped in *Kapton® Polyimide Film* for electrical insulation. Encapsulant, *Sylgard® 184 Silicone Elastomer* (chemical name *polydimethylsiloxane* elastomer), was poured over solar cell assembly till uniformly layered and left for 24 h to cure at room temperature. This ensured an appropriate optical coupling between the lenses and soldered cells assembly, as an adhesive as well as a protective coating from mechanical damages. Another thin layer over cured silicone ensures prevention against delamination at higher temperatures.

Perspex sheet (*cast Poly-methyl methacrylate*) was cut to form the walls and holes were drilled for the 6 mm screws. Aluminium plate (0.6 mm thick) was cut to size and glued to the Perspex walls using epoxy sealant. Silicone sealant was used to seal the top Aluminium plate onto the wall thickness. Further, the screwed walls were also sealed using the same sealant to ensure a leak-proof bonding between the surfaces and edges. Thermo-physical properties of components of the integrated BICPV–PCM system are highlighted in Table 2. Rubitherm® RT 42, (melting range: 38–43 °C) was used as the PCM for temperature regulation of the BICPV module.

2.3. Experimental procedure

The BICPV–PCM system was characterised at 0° from horizontal under the *Wacom Super Solar Simulator®* for providing highly collimated illumination. The schematic diagram of the experimental set up and the location of the selected temperature monitoring points are represented in Fig. 3. A set of four K-type thermocouples were attached to the back side of the BICPV module (top Aluminium plate of the system) using Aluminium adhesive tape (for improved conduction and accurate temperature measurements). Another set of four K-type thermocouples were attached to the inner side of the bottom Aluminium plate of the containment. The locations were chosen to study temperature variations across the centre and corners of the module for examining the extent of temperature distribution within the plates. The *I–V* characteristic evaluation of the module was recorded using *EKO MP-160i I –V* Tracer and *Keithley Model 2700* Digital Multimeter Data Acquisition and Datalogging System was used to simultaneously measure temperature. The data was recorded for over 2 h-period at an interval of 5 min. Ambient temperature and relative humidity were recorded using *Hygrometer testo 608-H1*.

3. Results and discussion

3.1. Electrical characterisation of the BICPV–PCM system

The short-circuit current (I_{SC}) and the open-circuit voltage (V_{OC}) are the two fundamental parameters of the *I–V* curve for a PV module. Both I_{SC} and V_{OC} are dependent on the incident irradiance and module temperature in such a way that change in I_{SC} and irradiance is almost directly proportional while change in V_{OC} is nominal. On the contrary, V_{OC} is inversely proportional to the module temperature causing significant reduction in electrical power at higher temperatures even though I_{SC} increases nominally [47]. Experimentally, it has been verified that an increase in module temperature leads to decrement in maximum output power (P_m) within the aluminium (thermal conductor) backed module. The BICPV–PCM module was illuminated by the solar simulator with 1000 W m^{-2} irradiance and aligned at 0° from the horizontal for a period of 145 min. I_{SC}, V_{OC} and P_m curves w.r.t. the elapsed time, for the BICPV system without and with PCM, were obtained as shown in Fig. 4(a)–(c) respectively. An increase in both, V_{OC} and P_m, was observed using PCM due to the inverse temperature relationship, while the I_{SC} showed proportional decrease. At the start of the experiments, the voltage improvement was only slightly higher in BICPV–PCM system, which continued to increase as the experiment preceded and similar behaviour, was observed for the difference in P_m. The average V_{OC} without PCM was 2.49 V which increased to 2.63 V with PCM, hence a 5.6% increase. As can be observed in Table 3, the minimum output $P_{m,}$ using PCM was

Table 2
Thermo-physical properties for various components of the BICPV–PCM system.

Thermo-physical properties of the components						
Component	**Solar cell**	**Concentrator**	**Back plate**	**Insulation**	**Encapsulation**	**PCM**
Material	Silicon	Crystal Clear® 200	Aluminium	Kapton® tape (polyimide)	Sylgard® 184 Silicone	RT-42®
Width (mm)	6	136	169	25	169	–
Length (mm)	115	120	160	3300	160	–
Thickness (mm)	0.3	170	0.6	0.065	0.5	–
Density (kg/m^3)	2329	1036	2700	–	1030	–
Thermal conductivity (W/m/K)	149	–	205	–	0.27	0.2
Molar heat capacity (J/mol/K)	19.79	–	–	–	1030	–
Latent heat capacity (kJ/kg)	–	–	–	–	–	174
Melting temperature (°C)	–	–	660	–	–	38–43
Max. operation temperature (°C)	–	–	–	180	–	90
Volume expansion (%)	–	–	–	–	–	12.5
Volume resistivity (Ωm)	–	–	–	1×10^{14}	–	–
Dielectric breakdown voltage (V)	–	–	–	7500	–	–
Temperature range (°C)		–	–	–	−45 to 200	−4 to 72

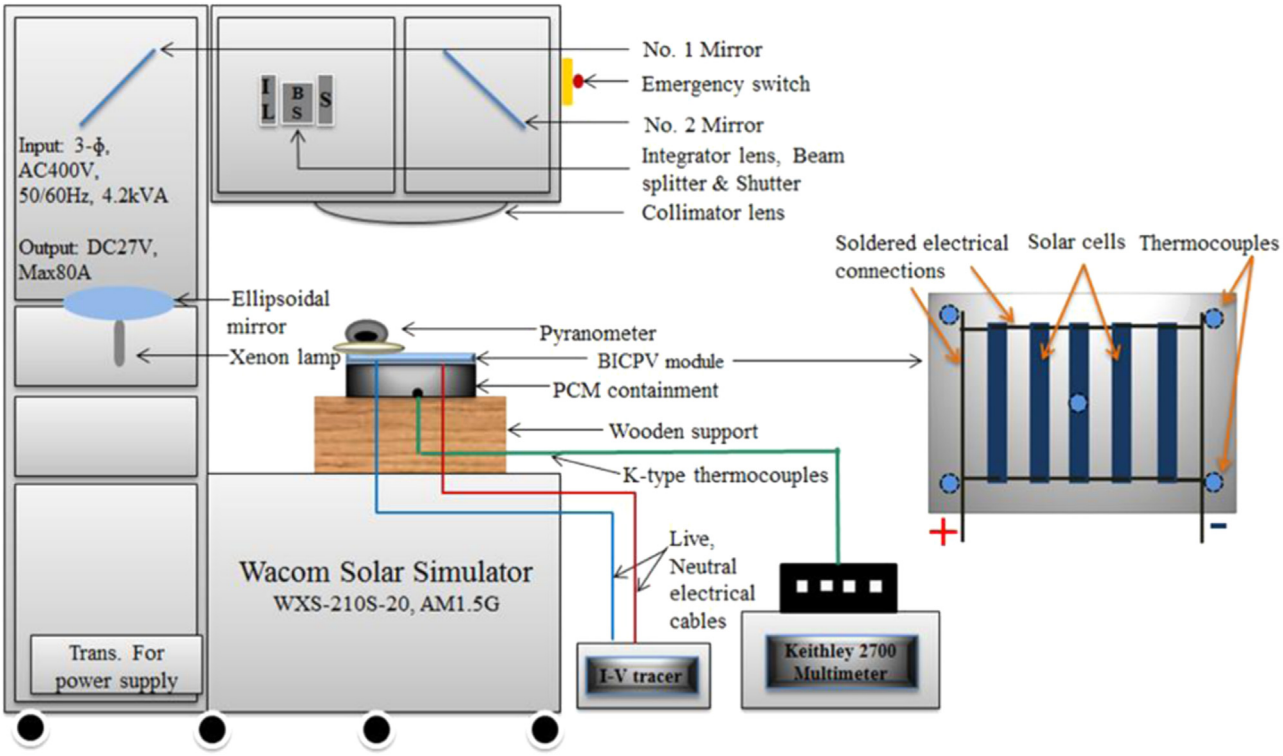

Fig. 3. Experimental set up for characterising BICPV and BICPV–PCM system showing temperature monitoring points for the thermocouples (rear side of top plate).

almost 17% higher than without PCM, which is due to thermal regulation of the module provided by the PCM. The maximum value of $P_{m,}$ was however higher for the non-PCM case (by 5%) due to the lower ambient temperature at the start-up. P_m with PCM overtakes P_m without PCM after 15 min of running the experiment. Similar to T_c fluctuations, P_m decreases sharply with PCM in the first 30 min (60 min without PCM) and stabilises later. The melting temperature range of the PCM used for the experiment could effect this duration. After 70 min of running the experiment, P_m stabilised (fluctuation < 8 mW) for the rest of the duration with PCM while without PCM, P_m stabilised for a while after 70 min but then started reducing further after 110 min (Fig. 4(c)). Overall, the average P_m without PCM was 581.7 mW while with PCM, it increased to 626.4 mW thereby showing a 7.68% relative efficiency improvement. The absolute electrical power conversion efficiency for the module without PCM cooling was observed as 6.48% while with the use of PCM in the system, it increased to 6.98%. In Fig. 4(d), a comparison has been made between the percentage change in P_m and the T_c at a frequency interval of 30 min whereby negative values indicates decline over a period of time. The current–voltage characterisations (I–V) of the system without and with PCM are shown in Fig. 4(e) and (f) respectively.

3.2. Effect of varying irradiance intensity

The experiment as described in the previous sections, was performed again for 120 min using various irradiance levels (500, 750 and 1200 W m^{-2}) to assess the effectiveness of PCM utilisation with respect to available irradiance. The effects of increasing irradiance intensity on PCM effectiveness and I_{SC}, V_{OC} and P_m are shown in Fig. 5(a)–(c) respectively. It is to be noted that the experiments were conducted for lesser duration, so a comparison has been drawn for about 125 min. As was expected, higher irradiance intensity led to an increase P_{m}. However, this increase in P_m was not directly proportional to the increase in irradiance using PCM, especially at higher intensities. The relative increase (calculated as a percentage figure) in electrical power using PCM with the BICPV system were recorded as 1.15% at 500 W m^{-2}, 4.20% at 750 W m^{-2} and 6.80% at 1200 W m^{-2}. It is worth noting that at 1200 W m^{-2}, the P_m increase with PCM was about 1% lesser than that at 1000 W m^{-2}, the reason for this could be inadequate PCM material thickness as well as melting range. The absolute average comparisons of $P_{m,}$ I_{SC} and V_{OC} without and with PCM are plotted in Fig. 5(e)–(g). The percentage variations in V_{OC} (and I_{SC}) were calculated as 1.6% (−1.3%) at 500 W m^{-2}, 2.4% (−0.5%) at 750 W m^{-2} and 3.9% (−3.8%) at 1200 W m^{-2}. The results indicate that this particular PCM has more pronounced effect for lower to medium levels and less effective for higher levels of irradiance which may be due to higher melting range of the PCM corresponding to heat generation in the BICPV panel at those intensities.

3.3. Temperature distribution

The BICPV module centre temperature (T_c) recorded at an interval of 5 min is plotted in Fig. 6(a). Comparing the average T_c attained by the non-PCM (50.1 °C) and the PCM attached (46.3 °C) systems, it was established that PCM utilisation reduced the average temperature by 3.8 °C in this instance. The duration for the experiment run could directly influence this difference; running the experiments for longer durations may stabilise the overall temperature with PCM absorbing all latent heat. The maximum T_c (49.2 °C with PCM and 55.2 °C without) was (3 °C with PCM and 5 °C without) higher than the average T_c in both the cases. A comparison between the change in P_m and T_c has been made in Fig. 4(d) for the two cases. As can be seen, during the first 30 min of running the simulator, the central temperature without PCM increased by 33 °C (24 °C with PCM) from the ambient 15 °C (24 °C with PCM) and caused a 18.6% (10.0% with

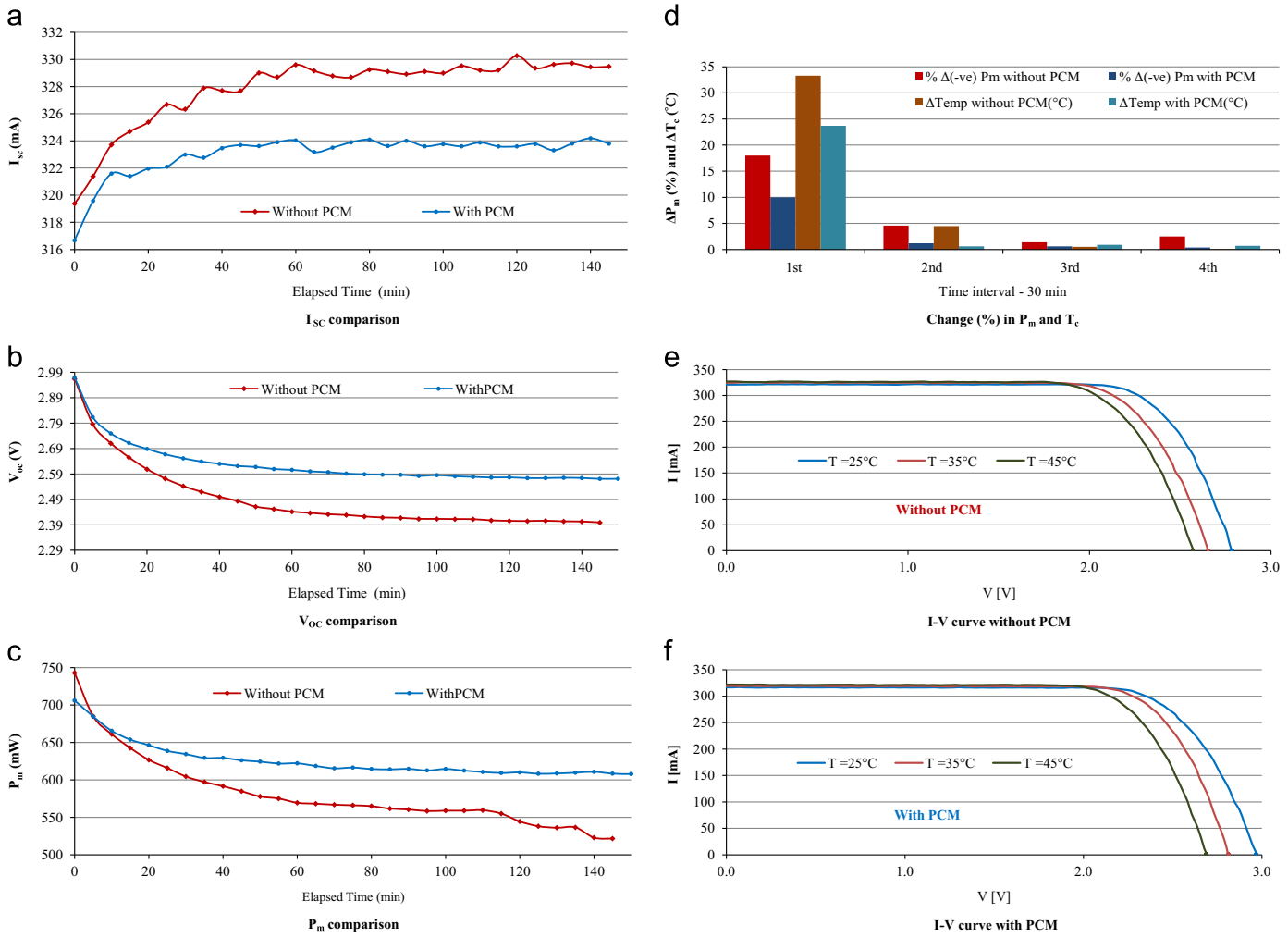

Fig. 4. Comparison of BICPV system parameters without and with PCM (RT42®) w.r.t. time (a) I_{SC}, (b) V_{OC}, (c) P_m, (d) percentage change in P_m and T_c at a frequency interval of 30 min, (e) *I–V* curve without PCM and (f) *I–V* curve with PCM (Inclination: 0°, Intensity: 1000 W m^{-2}).

Table 3
Important observed experimental data from the BICPV–PCM system output. (Negative sign indicates increase in the parameter value with the use of PCM).

	$T_{c,\ Min}$ (°C)	$T_{c,\ max}$ (°C)	$I_{SC,\ Min}$ (mA)	$I_{SC,\ Max}$ (mA)	$V_{OC,\ Min}$ (V)	$V_{OC,\ Max}$ (V)	$P_{m,\ Min}$ (mW)	$P_{m,\ Max}$ (mW)
Without PCM	15.0	55.2	319.4	329.7	2.4	2.96	521.5	742.9
With PCM	24.3	48.8	316.6	324.2	2.6	2.97	608.4	706.0
Change (%)	−62.0	11.6	0.9	1.7	−8.3	−0.3	−16.7	5.0

PCM) power loss. Similarly, during the second 30 min interval, T_c increased by 4.5 °C without PCM (0.6 °C with PCM) leading to power reduction by 4.6% (1.2% with PCM). In both the cases, increase in temperature after 60 min was only nominal. As highlighted in Table 3, using PCM reduces the maximum temperature, $T_{c,\ Max}$ of the module by 11.6% as compared to non-PCM system. The 62% increase in the minimum temperature, $T_{c,\ Min}$, with PCM usage in comparison to non-PCM system is due to the higher ambient temperature since the beginning of the experiment. The melting range of the PCM is 38–43 °C, which is slightly lower than the temperature at which the BICPV module temperature becomes nearly constant (46.5 °C) towards the end of 2 h of the experiment. The PCM containment bottom plate has been fabricated using Aluminium to gauge whether the quantity of heat available (after full-PCM melting), on the other end could be used for other regeneration purpose such as domestic water heating. This in turn could further improve the overall system efficiency by contributing in thermal processes alongside electrical efficiency improvement. As of now, there has only been a maximum temperature rise of 4 °C in the centre of the bottom plate with 24.4 °C as the average temperature. Running experiments for longer durations may however improve these figures. It may be concluded that using PCM, the temperature variation becomes more uniform over time and that the maximum fluctuations take place in the first 30 min of the entire duration and thereafter it is steadier than the non-PCM case, with only slight variations.

Highly non-uniform temperature distribution was also observed within the module without PCM. Relatively higher temperature were recorded under the module centre, lower towards the edges and lowest in the corners, which could be attributed to the edge effect or end losses due to interfacing with the surroundings. This internal temperature gradient may lead to local high-temperature hot spots within the module leading to efficiency loss and possible permanent degradation in the long run. The silicon solar cells in the module are soldered in series and the cell with the smallest output limits the overall output current, hence uniformity of temperature could again indirectly contribute to achieving higher overall electrical power output. It may be

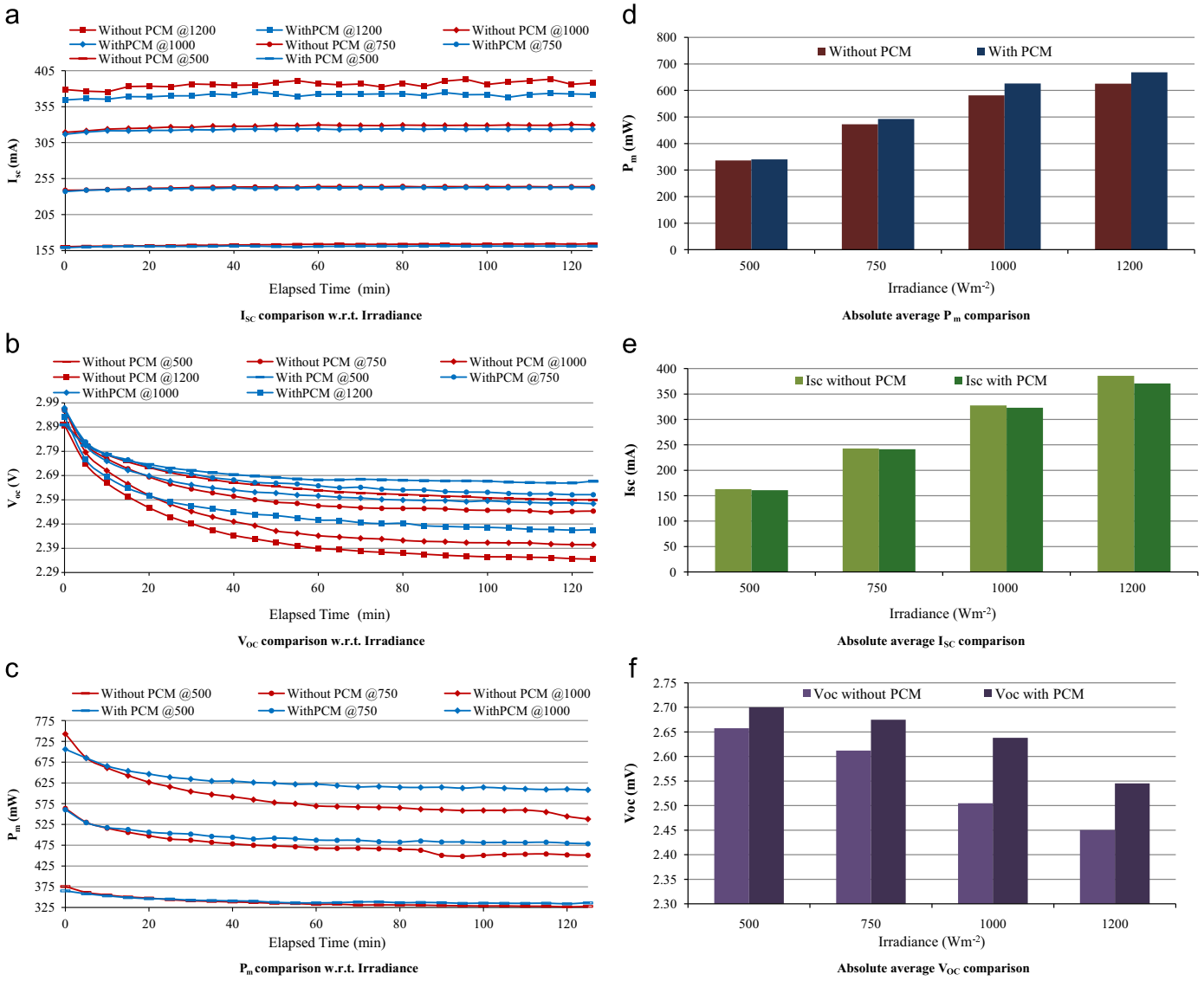

Fig. 5. Comparison of BICPV system parameters at various irradiance levels with and without PCM w.r.t. time; (a) I_{SC}, (b) V_{OC}, (c) $P_{m,}$ and absolute average value comparison of parameters; (d) P_m, (e) I_{SC} and (f) V_{OC} at various irradiance intensities (Inclination: 0°, Intensities: 500, 750, 1000 and 1200 W m^{-2}).

deduced that the use of PCM could also uniformalise the temperature throughout the BICPV module which may lead to prolonged module life. The fabricated BICPV module is unique and it differs from its previous counterparts [37,48–50] because instead of glass back-plate (for optical properties), Aluminium plate (for thermal conduction) was used for heat removal and possible recovery.

4. Conclusion

This paper experimentally investigates the feasibility of using PCM for thermal management of BICPV systems, which has not been reported so far. A PCM containment/heat sink was designed and developed and integrated with an in-house manufactured BICPV module. This BICPV–PCM system was tested in naturally ventilated module (without PCM) and then with PCM. An organic PCM (RT 42®) was used to regulate the aluminium back-plate temperature at 1000 W m^{-2} in the first instance. The stable BICPV temperature (46.5 °C) was achieved at a temperature slightly higher than the PCM maximum melting range (38–43 °C). A steep increase in temperature and corresponding reduction in maximum power was observed during the first 30 min of the experiment. This initial investigation resulted in a relative electrical efficiency improvement of 7.7% using PCM and relative V_{OC} improvement as 4.4% with PCM than with no PCM at 1000 W m^{-2}. Average temperature reduction of 3.8 °C was attained at the BICPV module centre integrated with PCM containment as compared to the non-PCM system. The test was performed at other irradiance levels (500, 750 and 1200 W m^{-2}) and the relative electrical efficiency improved by 1.15% at 500 W m^{-2}, 4.20% at 750 W m^{-2} and 6.80% at 1200 W m^{-2}. In the past, numerous studies have been performed on BIPV systems and have primarily focussed on the temperature and melt fraction with respect to time, (the PCM containment part of the system). In the present study, however, a thorough investigation on the effect of PCM cooling on the solar panel (BICPV side) including I_{SC}, V_{OC} and P_m output are also targeted. As yet, the proposed mathematical model for a BICPV–PCM system is the only optimised numerical model for designing such systems. In future, the experiments could be iterated for longer durations to explore PCM cooling characteristics. Studies on PCM containment bottom plate temperature rise could help in

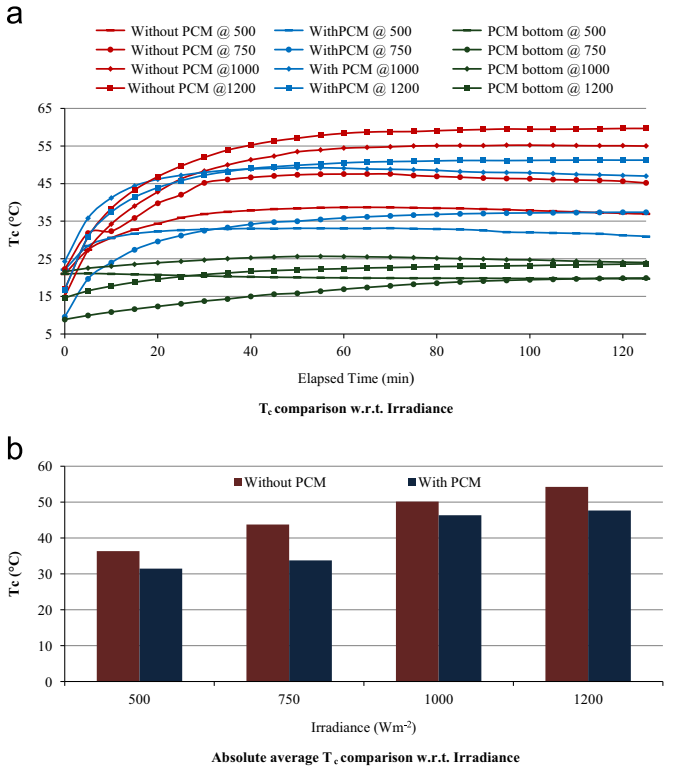

Fig. 6. Temperature variations at the centre of the BICPV system with and without PCM (RT42®) (a) measured at the rear of the BICPV panel (with and without PCM) and bottom of the PCM containment (PCM bottom), and (b) absolute average T_c at various irradiance intensities (Inclination: 0°, Intensities: 500, 750, 1000 and 1200 W m^{-2}).

assessing whether the rejected heat could be used for regeneration purposes. The experiment proves that the utilisation of PCM could contribute to effective thermal management of BICPV modules. However, building regulations, economic and environmental impact analysis could contribute to the further development of the technology.

Acknowledgement

The author would like to extend their gratitude to Mr. James Yule for mechanical workshop advice and assistance during the module fabrication. Funding from EPSRC-DST funded RESCUES project EP/K03619X/1 is gratefully acknowledged.

References

[1] V. Delisle, M. Kummert, A novel approach to compare building-integrated photovoltaics/thermal air collectors to side-by-side PV modules and solar thermal collectors, Sol. Energy 100 (0) (2014) 50–65.
[2] B. Norton, et al., Enhancing the performance of building integrated photovoltaics, Sol. Energy 85 (8) (2011) 1629–1664.
[3] D. Chemisana, Building Integrated Concentrating Photovoltaics: a review, Renew. Sustain. Energy Rev. 15 (1) (2011) 603–611.
[4] N. Sellami, Design and characterisation of a novel translucent solar concentrator (Ph.D. Thesis), Institute of Mechanical, Process and Energy Engineering, Heriot-Watt University, Edinburgh (2013), p. 307.
[5] L. Micheli, et al., Opportunities and challenges in micro- and nano-technologies for concentrating photovoltaic cooling: a review, Renew. Sustain. Energy Rev. 20 (2013) 595–610.
[6] A. Luque, A. Martí, Theoretical limits of photovoltaic conversion and new-generation solar cells, in: Handbook of Photovoltaic Science and Engineering, John Wiley & Sons, Ltd., 2011, pp. 130–168.
[7] M.J. Currie, et al., High-efficiency organic solar concentrators for photovoltaics, Science 321 (5886) (2008) 226–228.
[8] E. Casenove, et al., Assessment of a phase change material (PCM) system for moderating temperature rise of solar cells under concentrated sunlight, Adv. Sci. Technol. 74 (2010) 205–210.
[9] D. Du, J. Darkwa, G. Kokogiannakis, Thermal management systems for photovoltaics (PV) installations: a critical review, Sol. Energy 97 (0) (2013) 238–254.
[10] H. Baig, K.C. Heasman, T.K. Mallick, Non-uniform illumination in concentrating solar cells, Renew. Sustain. Energy Rev. 16 (8) (2012) 5890–5909.
[11] N. Yuksel, A. Avci, M. Kilic, A model for latent heat energy storage systems, Int. J. Energy Res. 30 (14) (2006) 1146–1157.
[12] B. Zalba, et al., Review on thermal energy storage with phase change: materials, heat transfer analysis and applications, Appl. Therm. Eng. 23 (3) (2003) 251–283.
[13] B. Gassenfeit, D. Brüggemann, Monolithic masonry with PCM for thermal management, Energy Procedia 48 (0) (2014) 1355–1364.
[14] M.H. Mahfuz, et al., Performance investigation of thermal energy storage system with phase change material (PCM) for solar water heating application, Int. Commun. Heat Mass Transf. 57 (0) (2014) 132–139.
[15] A. de Gracia, et al., Thermal analysis of a ventilated facade with PCM for cooling applications, Energy Build. 65 (0) (2013) 508–515.
[16] J.R. Turnpenny, D.W. Etheridge, D.A. Reay, Novel ventilation cooling system for reducing air conditioning in buildings. Part I: testing and theoretical modelling, Appl. Therm. Eng. 20 (11) (2000) 1019–1037.
[17] S. Kamali, Review of free cooling system using phase change material for building, Energy Build. 80 (0) (2014) 131–136.
[18] M. Koschenz, B. Lehmann, Development of a thermally activated ceiling panel with PCM for application in lightweight and retrofitted buildings, Energy Build. 36 (6) (2004) 567–578.
[19] K.A.R. Ismail, J.R. Henríquez, Thermally effective windows with moving phase change material curtains, Appl. Therm. Eng. 21 (18) (2001) 1909–1923.
[20] H. Mehling, et al., PCM-module to improve hot water heat stores with stratification, Renew. Energy 28 (5) (2003) 699–711.
[21] I. Cerón, J. Neila, M. Khayet, Experimental tile with phase change materials (PCM) for building use, Energy Build. 43 (8) (2011) 1869–1874.
[22] K. Nagano, et al., Study of a floor supply air conditioning system using granular phase change material to augment building mass thermal storage—heat response in small scale experiments, Energy Build. 38 (5) (2006) 436–446.
[23] F. Wang, et al., The novel use of phase change materials in refrigeration plant. Part 1: experimental investigation, Appl. Therm. Eng. 27 (17–18) (2007) 2893–2901.
[24] D.N. Nkwetta, F. Haghighat, Thermal energy storage with phase change material—a state-of-the art review, Sustain. Cities Soc. 10 (0) (2014) 87–100.
[25] A. Hasan, A.A. Sayigh, Some fatty acids as phase-change thermal energy storage materials, Renew. Energy 4 (1) (1994) 69–76.
[26] M.M. Farid, et al., A review on phase change energy storage: materials and applications, Energy Convers. Manag. 45 (9–10) (2004) 1597–1615.
[27] G. Fang, F. Tang, L. Cao, Preparation, thermal properties and applications of shape-stabilized thermal energy storage materials, Renew. Sustain. Energy Rev. 40 (0) (2014) 237–259.
[28] L. Fan, J.M. Khodadadi, Thermal conductivity enhancement of phase change materials for thermal energy storage: a review, Renew. Sustain. Energy Rev. 15 (1) (2011) 24–46.
[29] A. Sarı, Form-stable paraffin/high density polyethylene composites as solid–liquid phase change material for thermal energy storage: preparation and thermal properties, Energy Convers. Manag. 45 (13–14) (2004) 2033–2042.
[30] A. Sarı, A. Karaipekli, Thermal conductivity and latent heat thermal energy storage characteristics of paraffin/expanded graphite composite as phase change material, Appl. Therm. Eng. 27 (8–9) (2007) 1271–1277.
[31] Z. Ling, et al., Review on thermal management systems using phase change materials for electronic components, Li-ion batteries and photovoltaic modules, Renew. Sustain. Energy Rev. 31 (0) (2014) 427–438.
[32] Z. Rao, S. Wang, A review of power battery thermal energy management, Renew. Sustain. Energy Rev. 15 (9) (2011) 4554–4571.
[33] S. Kalaiselvam, R. Parameshwaran, S. Harikrishnan, Analytical and experimental investigations of nanoparticles embedded phase change materials for cooling application in modern buildings, Renew. Energy 39 (1) (2012) 375–387.
[34] S.M. Hasnain, Review on sustainable thermal energy storage technologies, Part I: heat storage materials and techniques, Energy Convers. Manag. 39 (11) (1998) 1127–1138.
[35] N. Sarmah, B.S. Richards, T.K. Mallick, Design, development and indoor performance analysis of a low concentrating dielectric photovoltaic module, Sol. Energy 103 (0) (2014) 390–401.
[36] T.K. Mallick, et al., The design and experimental characterisation of an asymmetric compound parabolic photovoltaic concentrator for building façade integration in the UK, Sol. Energy 77 (3) (2004) 319–327.
[37] H. Baig, et al., Numerical modelling and experimental validation of a low concentrating photovoltaic system, Sol. Energy Mater. Sol. Cells 113 (2013) 201–219.
[38] A. Sharma, et al., Review on thermal energy storage with phase change materials and applications, Renew. Sustain. Energy Rev. 13 (2) (2009) 318–345.
[39] V.R. Voller, Fast implicit finite-difference method for the analysis of phase change problems, Numer. Heat Transf. Part B: Fundam. 17 (2) (1990) 155–169.
[40] S.V. Patankar, Numerical heat transfer and fluid flow. Von S.V. Patankar. Hemisphere Publishing Corporation, Washington – New York – London.

McGraw Hill Book Company, New York 1980. 1. Aufl., 197 S., 76 Abb., geb., DM 71,90, Chem. Ing. Tech. 53 (3) (1981) 225.
[41] M.M. Farid, R.M. Husian, An electrical storage heater using the phase-change method of heat storage, Energy Convers. Manag. 30 (3) (1990) 219–230.
[42] L. Aelenei, et al., Thermal performance of a hybrid BIPV–PCM: modeling, design and experimental investigation, Energy Procedia 48 (0) (2014) 474–483.
[43] M.C. Browne, B. Norton, S.J. McCormack, Phase change materials for photovoltaic thermal management, Renew. Sustain. Energy Rev. 47 (0) (2015) 762–782.
[44] A. Hasan, et al., Evaluation of phase change materials for thermal regulation enhancement of building integrated photovoltaics, Sol. Energy 84 (9) (2010) 1601–1612.
[45] M.J. Huang, P.C. Eames, B. Norton, Thermal regulation of building-integrated photovoltaics using phase change materials, Int. J. Heat Mass Transf. 47 (12–13) (2004) 2715–2733.
[46] M.J. Huang, P.C. Eames, B. Norton, Phase change materials for limiting temperature rise in building integrated photovoltaics, Sol. Energy 80 (9) (2006) 1121–1130.
[47] M. Mattei, et al., Calculation of the polycrystalline PV module temperature using a simple method of energy balance, Renew. Energy 31 (4) (2006) 553–567.
[48] N. Sellami, T.K. Mallick, Optical characterisation and optimisation of a static window integrated concentrating photovoltaic system, Sol. Energy 91 (0) (2013) 273–282.
[49] N. Sellami, T.K. Mallick, Optical efficiency study of PV crossed compound parabolic concentrator, Appl. Energy 102 (0) (2013) 868–876.
[50] T.K. Mallick, P.C. Eames, B. Norton, Using air flow to alleviate temperature elevation in solar cells within asymmetric compound parabolic concentrators, Sol. Energy 81 (2) (2007) 173–184.